A single-coil-based method for electromagnetic interference reduction in point-of-care low field MRI systems

Parsa, J.; O'Reilly, T.; Webb, A.

Journal of Magnetic Resonance 346 (2023) 107355

Contents lists available at ScienceDirect

Journal of Magnetic Resonance

journal homepage: www.elsevier.com/locate/jmr

A single-coil-based method for electromagnetic interference reduction in point-of-care low field MRI systems

Javad Parsa [a,b], Thomas O'Reilly [b], Andrew Webb [b,*]

[a] Percuros BV, Leiden, the Netherlands
[b] Department of Radiology, Leiden University Medical Center, 2333 ZA Leiden. the Netherlands

ARTICLE INFO

Article history:
Received 6 February 2022
Revised 25 November 2022
Accepted 3 December 2022
Available online 7 December 2022

Keywords:
Point-of-care MRI
Electromagnetic interference
Passive RF Shielding
Quadrature mode birdcage
Halbach magnet

ABSTRACT

One of the main challenges for point-of-care (POC) MRI systems is electromagnetic interference (EMI), since such systems are intended for use outside conventional Faraday-shielded rooms. Many methods have been proposed based on EMI detection via sensors external to the MRI system, followed by different types of signal processing to reduce artifacts in the image. Although these methods can be very effective, they do increase the complexity of the overall system, and introduce more potential failure points for systems designed for challenging environments. In this work we introduce a new method that does not require external sensors, but rather uses the "MR-silent" mode of an RF coil to detect the EMI, followed by simple subtraction from the signal from the "MR-active" mode. This method can be performed post-acquisition if there are two receive channels available, or as demonstrated here can operate with a single-channel receive detection system with the addition of a simple passive 180° power splitter/combiner into the receive chain. Proof-of-concept in vivo results show that a reduction in the standard deviation of the EMI up to ~ 97 % is possible, with average values ~ 90 %.

1. Introduction

Low field point-of-care (POC) MRI systems are generating increasing interest, with a number of academic and commercial systems being produced in the past few years [1–8]. These portable POC systems can be utilized in hospital intensive care units (ICUs) and emergency departments (EDs) [9,10,8,11], or can be designed for locations, such as rural areas, with a lack of access to conventional MRI.

In addition to the intrinsic low signal-to-noise ratio (SNR), one of the major challenges in POC MRI is that the systems should be designed to operate outside the usual RF shielded environment (Faraday shielded room). Electromagnetic interference (EMI) created either by equipment close to the scanners or consisting of general environmental EM noise can cause artifacts which render images non-diagnostic. For portable MRI devices, some degree of shielding can be built directly around the scanner. However, at least one side of the scanner cannot be shielded to allow patient access. In addition to this opening, the human body acts as an antenna for any external EMI [12] and "guides" this EMI into the imaging region. A conductive mesh cloth can be draped over the patient to reduce the body antenna effect [13], but this set-up can be somewhat uncomfortable and relies on very good contact with any local shielding structures. As reported by Srinavas et al. [14] this approach works in ~ two-thirds of cases on their yoked 47 mT system, and this number is similar in our experience on a 50 mT Halbach-based system [13].

Many different methods to reduce EMI for MRI/NMR have been explored in the past [15–20]. Most approaches are applied in post-processing by using data from external sensors, such as additional RF coils. A method by Srinavas et al. [14] was recently implemented on 47.5mT and 80 mT low field scanners systems which have multiple receive channels. This method proposes an approach to dynamic EMI correction using data acquired simultaneously during the scan from EMI detectors external to the MR coil. The model can dynamically adjust to time-varying external noise sources, and resulted in up to 76 % EMI reduction in the presence of broadband sources, and 97 % for structured EMI. A machine-learning approach for EMI cancellation has been presented by Liu et al. [7] for their low-cost, shielding-free brain MRI scanner based on a two-pole 0.055 T samarium-cobalt (SmCo) permanent magnet. Ten EMI sensing coils were placed in the vicinity of the transmit and receive coils, underneath the patient bed, and inside the electronics cabinets. In the "dead time" of the sequence, when RF pulses were not being transmitted nor signals received, any EMI interference detected by the sensing coils and MR receive coil were

* Corresponding author.
E-mail address: a.webb@lumc.nl (A. Webb).

https://doi.org/10.1016/j.jmr.2022.107355
1090-7807/

recorded, and used to train a five-layer convolutional neural network (CNN) model. This model was then used to predict the EMI signal component in the MRI receive coil based on the signals picked up by the sensing coils: this EMI component was then subtracted from the image. The authors reported EMI levels within 5 % of those obtained when using a Faraday cage.

Although these approaches have been shown to be very effective, one of the intrinsic disadvantages of the (multiple) external detector approach is the added system complexity and the requirement for a multi-channel receiver. This is particularly relevant in the context of challenging working environments which introduce more potential failure points. In this current work, we propose a new approach which can be used on MRI systems (including most open and portable systems) with a transverse B_0 field without the need for external sensors. This approach uses a circularly-polarized RF coil, with one of the ports being "MR-inactive" and detects only the EMI, whereas the other one detects both MR signal and EMI. Signal combination can be performed in software if two separate receiver channels are available, or in hardware (as shown here) if only one receiver channel is available, both of which result in reduction in the EMI component. Phantom and in vivo images with and without EMI have been acquired to evaluate this approach.

2. Material and methods

2.1. Halbach magnet array and data acquisition system

All data were acquired on a custom-built 50 mT (2.15 MHz) Halbach-based MRI scanner described in detail previously [5]. The magnet is 50.6 cm long and has a 27 cm diameter bore. A Magritek Kea2 spectrometer (Aachen, Germany) with a single receive channel, was used. The spectrometer has a built-in transmit/receive switch and preamplifier. The entire setup is placed inside a Faraday cage constructed from aluminum extrusion and 2 mm thick aluminum plates.

2.2. RF coil and hardware setup

Fig. 1 shows the concept of the EMI-cancellation scheme. The RF setup consists either of a single coil with inherent circular polarization, e.g. a quadrature birdcage, or two coils with orthogonal B_1-field orientations, such as two saddle coils rotated 90° with respect to one another. In either case, one of the B_1 field directions is orthogonal to B_0, and the other is co-incident. In this paper we use a quadrature birdcage due to the ease of designing the circularly polarized modes to have exactly equal sensitivities. The B_0-orthogonal (MR-active) channel is sensitive to the MR signal and any EMI present, while the B_0-parallel (MR-inactive) channel detects only the EMI. The birdcage coil is not shielded, but the inner bore of the magnet has a thin floating copper shield to minimize gradient/RF coil interactions: this reduces the efficiency of the RF coil via the induction of mirror currents, but this reduction is relatively small (<10 %) given that there is an ~ 5 cm gap between coil and shield.

There are two possible ways to combine the channel/coil signals. If the acquisition system has multiple receive channels, then the signals can be received separately and then the noise peak can be subtracted in software. Alternatively, if only a simpler one-channel acquisition system is available, then the signals can be directly subtracted in hardware using, for example, a 180° power splitter/combiner. In this work we adopt the latter hardware-based approach in line with making the overall cost and complexity of the system as low as possible. The 180° power splitter/combiner was placed directly in front of the input to the transmit/receive switch of the Kea, as shown in Fig. 1.

2.3. RF coil design and 180° power splitter/combiner characterization

A 16-leg low-pass transmit/receive birdcage for knee or calf muscle imaging was constructed on a plexiglass cylinder using copper tape, 13 mm wide and 0.06 mm thick. The coil dimensions were 19 cm long (measured between the centre of the end ring conductors) and 16 cm in diameter. Non-magnetic tuning capacitors with values 12,456 pF were placed in each leg. The reflection coefficient parameters (S-parameters), isolation between two ports, and the quality (Q) factors of the coil were measured with a network analyser (S5048, 20 kHz-4.8 GHz, Copper Mountain Technologies). The S_{11} values for each port were < -25 dB, and the isolation between ports was > 25 dB. The Q-value of the coil loaded with a human leg was ~ 45 (the two channels had slightly different values, one 47 and the other 43), with negligible frequency shift when the leg was placed inside the coil. A 180° power splitter/combiner (SBTCJ-1 W+, Mini-Circuits, NY, USA) was placed inside an aluminum shielded box. Measurements on the 180°

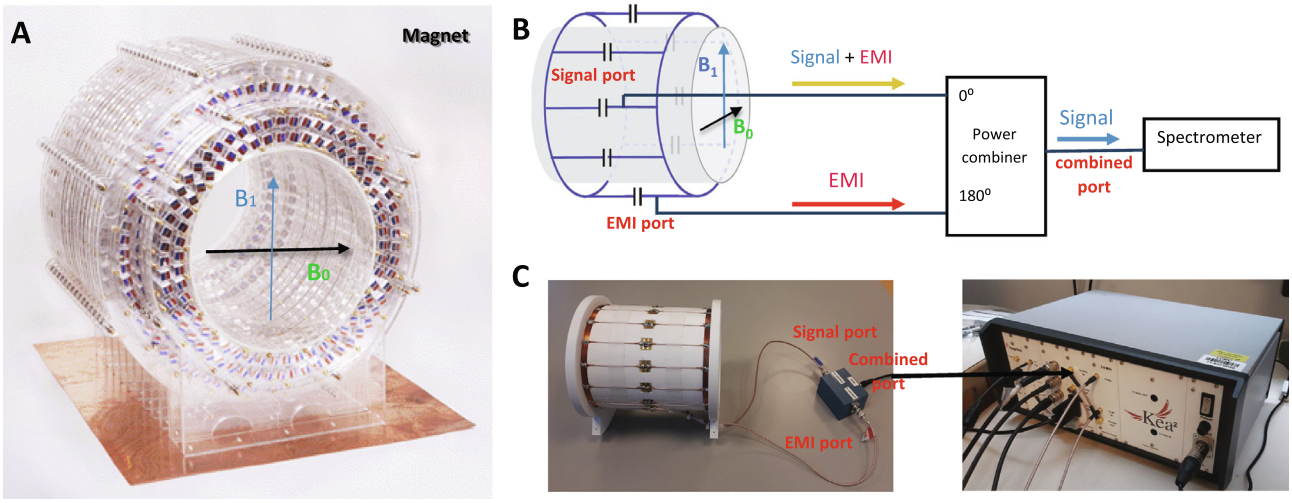

Fig. 1. Photographs of the physical setup and a schematic of the method used to cancel EMI. The RF coil has two orthogonal receive ports, one of which is orthogonal to B_0 and the other parallel. Signals from the MR-inactive and MR-active ports are combined with a 180° power splitter/combiner to reduce the EMI. The output of the splitter/combiner feeds into the transmit/receive switch of the spectrometer.

power splitter/combiner at 2.15 MHz gave an overall 3.2 dB insertion loss (3 dB intrinsic + 0.2 dB resistive loss), 0.5^0 phase unbalance, and > 25 dB inter-channel isolation.

2.4. Phantom and in vivo imaging experiments

To determine the performance of the EMI-cancellation concept four different imaging setups were used:

1) the normal operating mode in which the subject's torso is covered by a conductive blanket (Holland Shielding Systems, Dordrecht, the Netherlands) and the remaining sides of the aluminum Faraday cage are all closed,
2) unshielded state, not using a conductive blanket and the Faraday shield open at the front and back. The EMI comes from the environmental background, which in our hospital was measured to be essentially broadband with no specific frequencies within our measurement bandwidth,
3) unshielded state (no blanket, open Faraday shield) with narrowband EMI present, produced by a tuned helical resonator connected to a function generator (33500 Series waveform generators, Agilent Technologist, US) placed in random locations around the magnet to produce a single frequency 10 mV peak-to-peak sine wave at 2.15 MHz.
4) unshielded state (no blanket, open Faraday shield) with broadband EMI present at a maximum amplitude of 40 mVp-p produced by the same function generator over a frequency range 0–3 MHz.

In each of these set-ups the EMI is assumed to be non-directional in terms of polarization. For each of these setups, the following data were acquired. First, with only the MRI signal port connected to the spectrometer, second with only the EMI port connected, and third the full setup with both the signal and EMI ports connected via the 180° power splitter/combiner to the spectrometer (Fig. 1). For each scan, the 90° pulse was separately calibrated, but all other imaging parameters remained the same. Since, for a single channel receiver, the three measurements must be acquired separately in order to capture the separate images, the EMI port data were not collected for the in vivo scans in order to reduce the total scan time for which the volunteer had to be in the magnet.

Since in all practical in vivo imaging situations a large part of the body extends out of the Faraday shield, and conducts external noise into the coil via the body-antenna effect, we constructed a realistic phantom which also extends a significant way outside of the aluminum Faraday shield. Such a "leg phantom" was constructed, consisting of an 11 cm diameter, 90 cm long tube of water, doped with 1.5 g/l NaCl.

A 3D turbo spin-echo (TSE) sequence was used for all scans. The sequence parameters were TR/TE 1000 ms/15 ms, echo train length (ETL) 20, field-of-view (FOV) 150 × 150 × 300 mm, 2 × 2 × 5 mm spatial resolution, acquisition bandwidth 20 kHz. For in-vivo scanning, the calf muscles of two male volunteers were imaged (data for the first are shown in Fig. 2, and for the second in Figs. 3, 4 and 5). Written consent was obtained from each volunteer. A TSE sequence was used with TR/TE 250 ms/15 ms, ETL 4, FOV 160 × 160 × 200 mm, 2 × 2 × 5 mm spatial resolution, acquisition bandwidth 20 kHz, and two signal averages. The readout direction was along the bore of the magnet (x-direction) and the two phase-encoding dimensions were transverse to the bore (z- and y-directions).

For quantitation, the SNR was calculated by dividing the mean signal intensity in a region-of-interest (ROI) drawn around the entire calf divided by the standard deviation (σ) of the noise measured in an area of the image with no signal. To quantify the reduction of EMI we use the same formulation as Srinivas et al. [14],

$$EMI_{reduction} = \frac{|\sigma_{UN} - \sigma_C|}{\sigma_{UN}} \times 100\%$$

where σ_{UN} and σ_C are the standard deviations of an EMI region in the subtracted and original images, respectively, measured outside the phantom/calf muscle.

3. Results

Fig. 2 shows phantom and in vivo imaging results acquired with full shielding and no external EMI applied: these data sets are used as a baseline with which to compare the other setups. For both setups the ratio of the signal from the signal port to that of the EMI port was 45:1, representing a greater than 97 % isolation between the ports. The SNR from the combined port was reduced by ~ 40 % compared to that of the signal port without the combiner present, due to the inherent 3 dB reduction in signal from the 180° hybrid, in addition to the 0.2 dB resistive loss. There is a measured ~ 35 % loss in SNR for the in vivo experiment (see Table 1).

Fig. 3 shows in vivo results with the conductive cloth removed and the Faraday shield open. As expected there is an overall reduction in the SNR due to more noise being introduced via the "human antenna" effect: in this case the SNR is reduced by ~ 20 %. This number can be quite variable between subjects, typically between 5 and 40 % in our experience similar to numbers reported by Srinivas et al. [14], and depends how well the system is shielded and grounded which is challenging due to the flexible nature of the cloth.

Fig. 4 shows results using, separately, the single frequency and the broadband sources with the leg phantom, without the shielding cloth, at five different locations with respect to the magnet entrance (10 cm distance in each case). Very similar EMI reductions were obtained from each of the positions.

Fig. 5 shows results with the single frequency EMI source located near the volunteer's head and close to the scanner. The results averaged over five central slices in the 3D data set showed an average 96.7 % $EMI_{reduction}$ for the in vivo images.

Fig. 6 shows the results from the application of a broadband 0–3 MHz noise source. The average EMI reduction factor was 90 % averaged over the central five slices.

Table 1 shows a summary of the in vivo measurements in terms of SNR and $EMI_{reduction}$.

4. Discussion

A new very simple EMI cancellation method has been introduced for MRI systems with a transverse B_0 field and has been tested on a 50 mT Halbach-based portable MRI system for in vivo imaging in unshielded conditions, with and without external EMI. The main advantages of this method over existing ones are that it can be performed on data acquisition systems with only a single receive channel and does not require the added complexity of additional sensors, and that the EMI signal is acquired at the exactly same physical location as the MRI signal and with the same sensitivity. The results shown here demonstrate up to 97 % EMI reduction for in vivo imaging. The residual EMI we attribute to the slightly different Q-values of the two channels, which are probably the result of slight construction asymmetries.

The use of a transverse resonator rather than an axial resonator does lead to a loss in intrinsic sensitivity. The transmit (B_1^+) and, by reciprocity, the receive (B_1^-) fields of a solenoid are higher than those of an equivalently-sized birdcage [21]. We measured the respective 90° pulse powers and SNR for a small phantom inside the coil and found that there is almost exactly a factor-of-two dif-

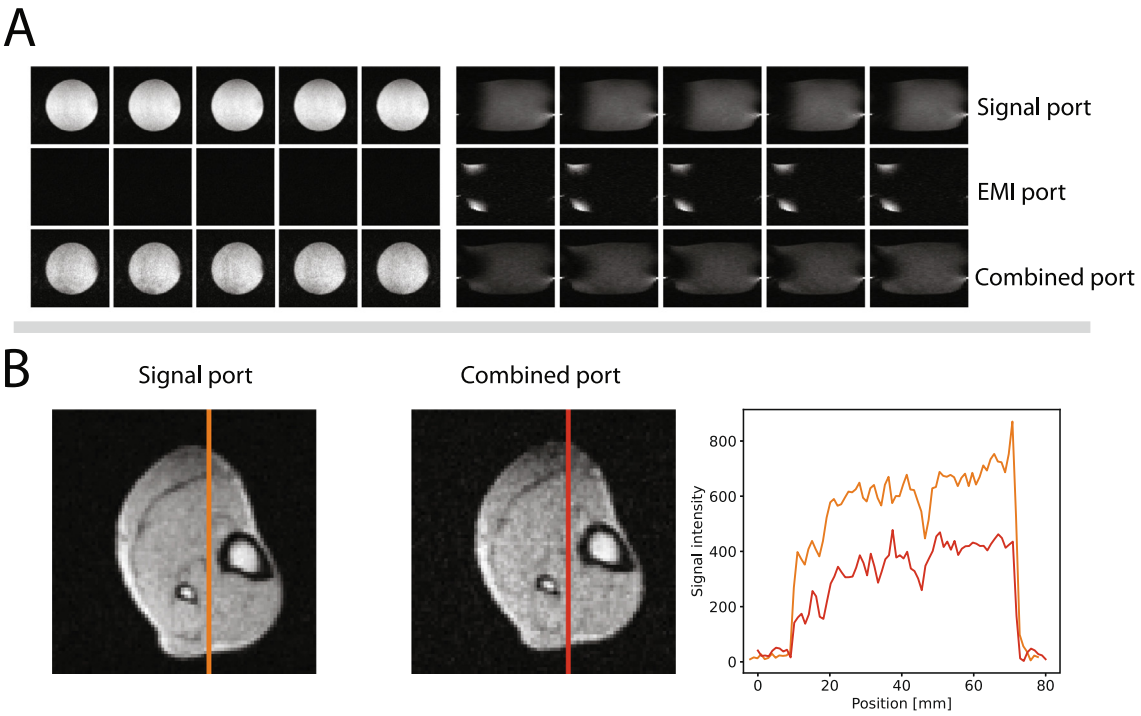

Fig. 2. A: Three axial (left) and sagittal (right) slices from the leg phantom. B: The central-slice in vivo images from the signal port and the combined port with (right) corresponding 1D-profiles. The conducting blanket is present, the Faraday shield is closed on three sides and top/bottom, and there is no external EMI applied.

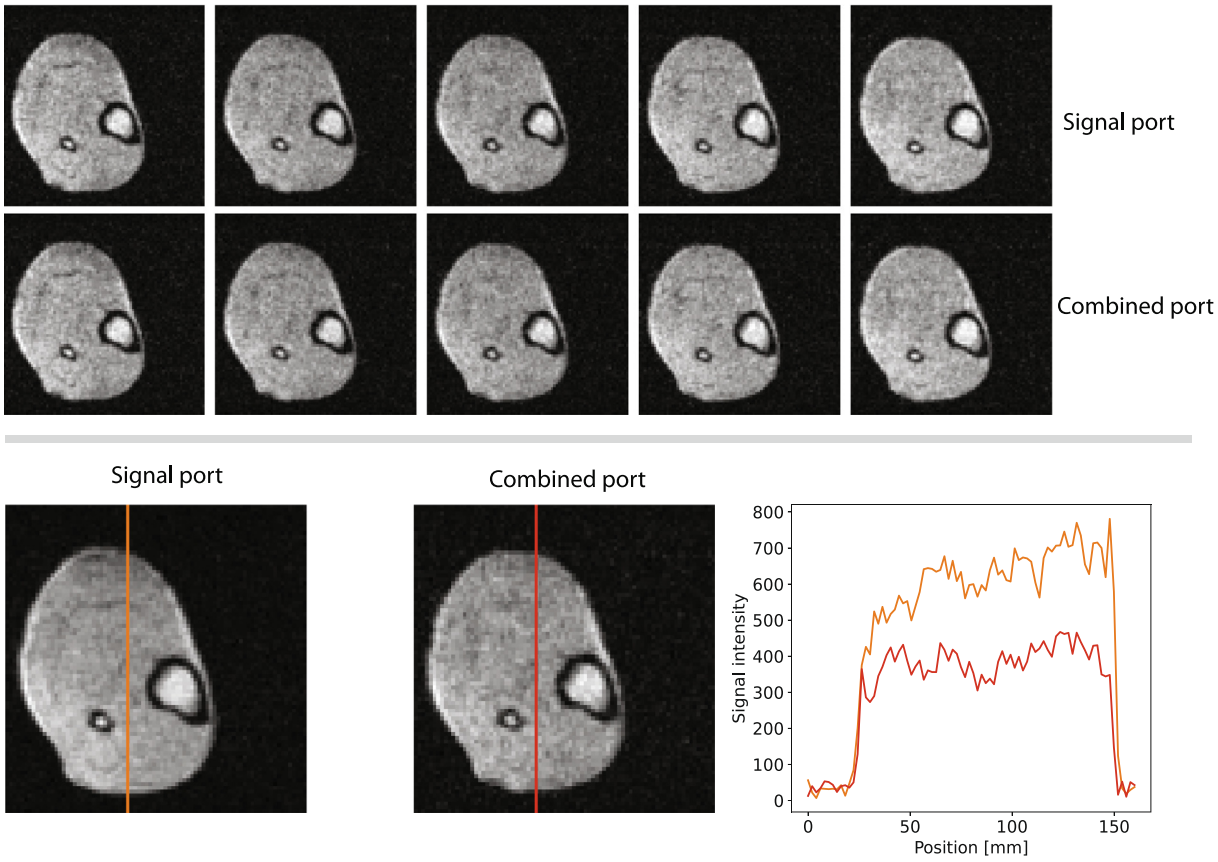

Fig. 3. In vivo imaging results without the shielding cloth and with the Faraday shield open.

ference. However, we also performed measurement which shows that the solenoid is much more sensitive to external noise when the sample/subject extends out of the Faraday shield. Using the long leg phantom, with no shielding cloth, the standard deviation of the noise for the solenoid was more than ten times larger than for the birdcage, meaning that the overall SNR was four times less.

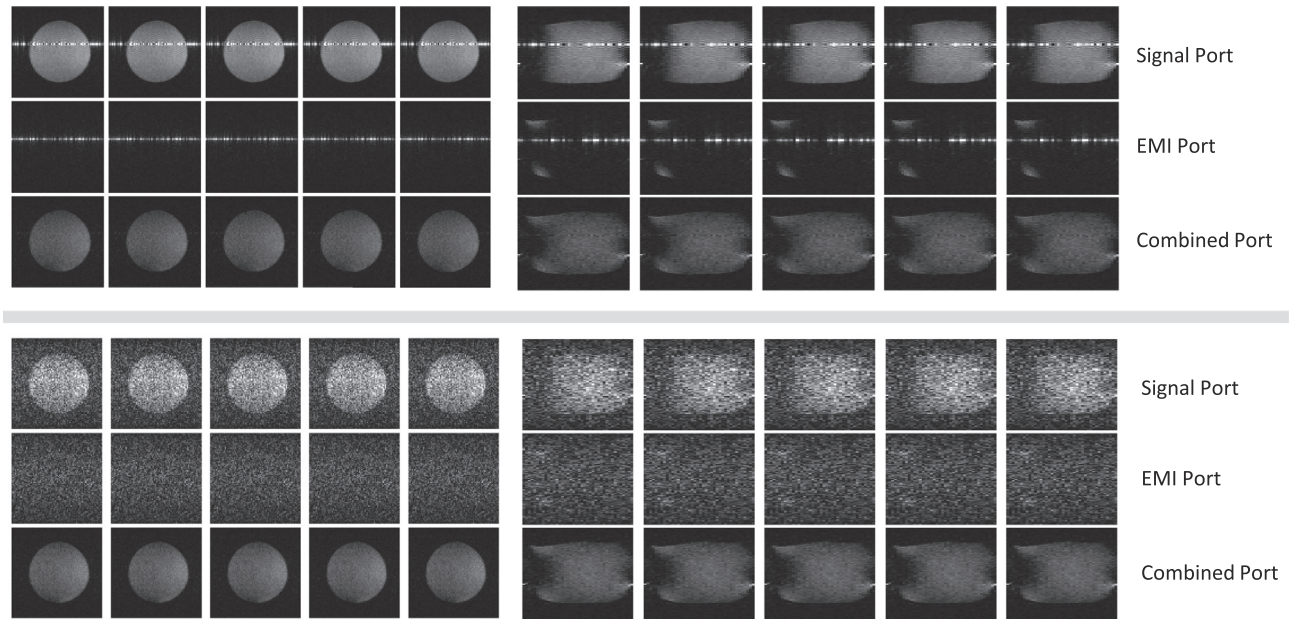

Fig. 4. Transverse (left) and sagittal (right) central slices from the leg phantom obtained using single frequency (top) and broadband (bottom) EMI. Five different locations of the EMI source are used: left-to-right: directly in front, 10 cm above, 10 cm to the left, 10 cm below and 10 cm to the right of the magnet bore. The EMI reduction factors are 91.3, 93.3, 91.8, 91.4 and 92.2 %, respectively.

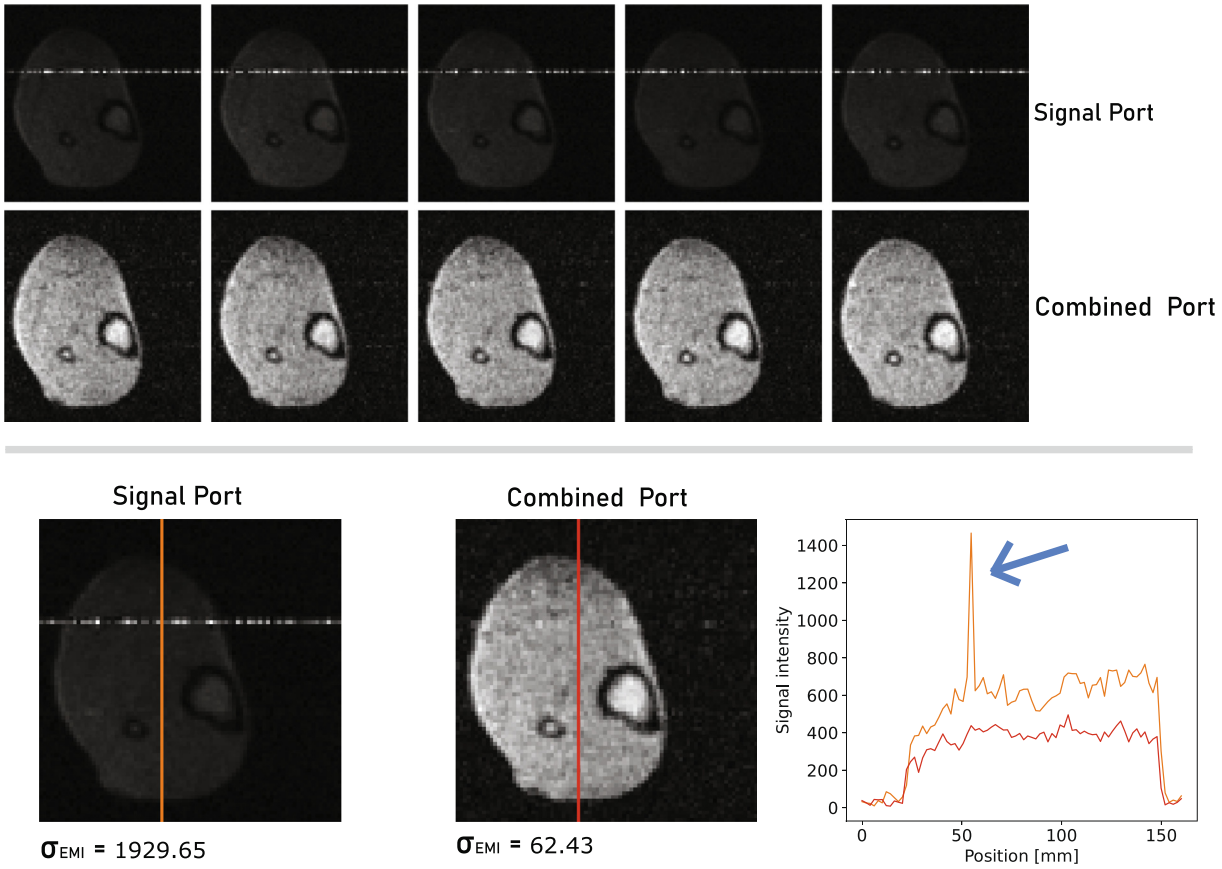

Fig. 5. In vivo experiments with a single frequency EMI apparent as the line through the image in the phase encoding direction. No conductive cloth was used and the Faraday shield was open. On the right, the peak on the orange line, which is highlighted with a blue arrow, shows the EMI present in the signal port measurements. The standard deviation of the EMI (σ_{EMI}) was measured over the EMI line in a background region.

In order to put the EMI reductions in context to "perfect" shielding, we also performed scans using broadband EMI with a small phantom inside the RF coil so that the Faraday shield could be closed on all sides. Comparing the EMI level with that acquired with one of the ends of the shield removed gave a reduction in EMI of $\sim$ 93 %. Therefore, the method used here achieves approxi-

Table 1
SNR and EMI reduction measurements.

	In vivo			
	Shielded	**Unshielded**	**Unshielded + single frequency EMI**	**Unshielded + Broadband EMI**
SNR (signal port)	15.4 ± 0.3	12.7 ± 0.4	11.7 ± 0.5	–
SNR (combined port)	10.0 ± 0.2	8.6 ± 0.1	8.5 ± 0.3	7.9 ± 0.4
$EMI_{reduction}$	–	–	96.7 ± 0.7	91.2 ± 0.9

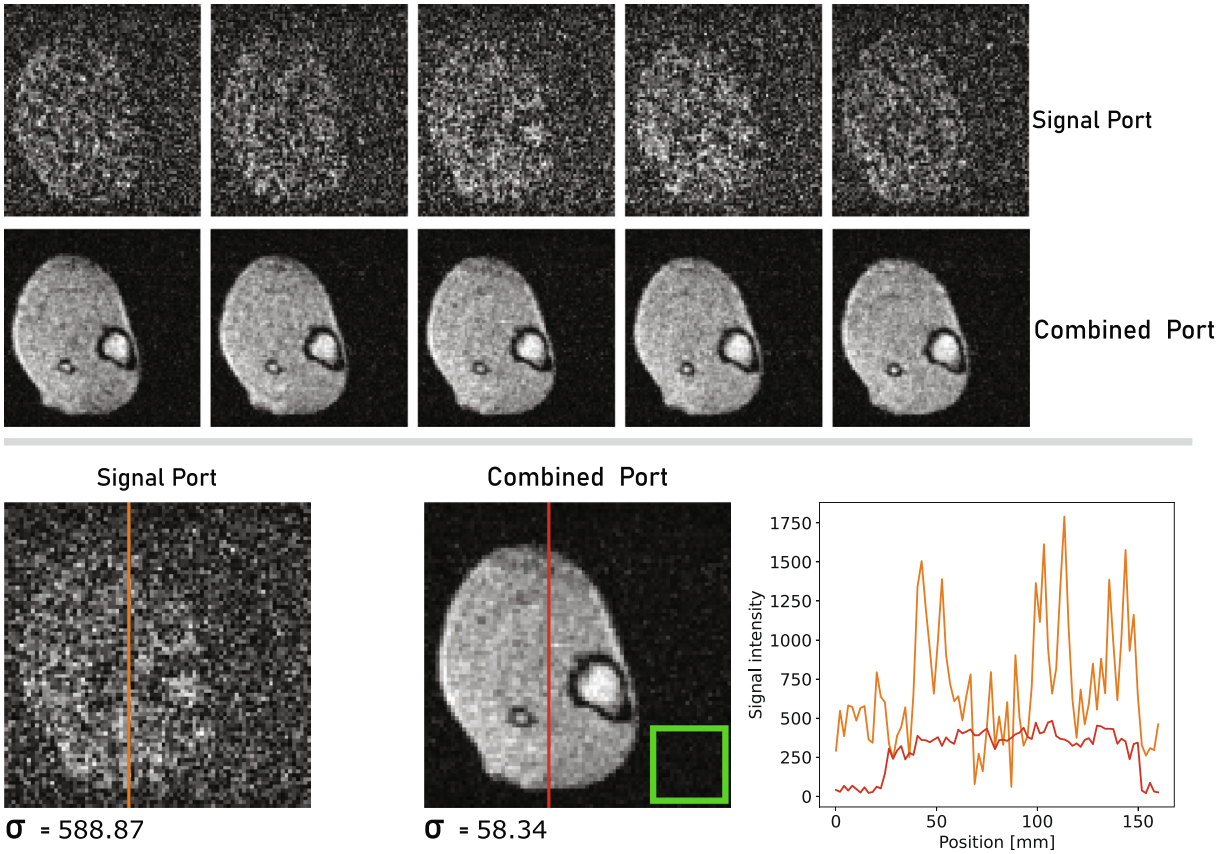

Fig. 6. In vivo and phantom results using an external 0–3 MHz broadband EMI noise source with no conductive cloth and Faraday shield open. The green rectangle shows the region of interest that was used to measure σ_{EMI}.

mately the same level as a closed Faraday cage, which of course is not possible in practise for in vivo scanning.

The requirement that the EMI port is parallel to the B_0 field is fulfilled in the experiments performed here, but if the imaging field-of-view is sufficiently large, then the direction of B_0 will deviate from being along the z-axis as displayed in Fig. 1. However, this would represent regions of the magnet in which the B0 homogeneity was so poor as to be effectively unusable. The bandwidth of the RF coil means that any regions where the transverse B_0 field varies by more than ~ 20 kHz cannot be excited, and this limits the effective imaging volume of the system.

If the spectrometer only has a single receive channel, as for the data presented here, there is an intrinsic loss in SNR, compared to an image acquired in the absence of any EMI, by a factor of ~ 40 % due to the process of signal combination in the 180° power splitter/combiner. Therefore, it is important to decide whether the EMI is the limiting factor in scanning, or whether a very low level of EMI can be tolerated and acquire the image with higher SNR. However, if a two-channel receiver is available then this loss can be eliminated. The method, as presented here, is also sensitive to the polarization of the EMI source. As mentioned in the text, all of the EMI sources in this study were non-directional. However, if there is a high degree of polarization then the sensitivities of the two ports of the RF coil to the EMI may be very different, and cancellation will be incomplete. In our experience within the hospital, we rarely encounter this situation, but if it does occur then this approach could be combined with those involving external sensors, such as directional loops, oriented in different directions so that a subset of them is sensitive to the EMI irrespective of its polarization.

5. Conclusion

A new EMI cancellation method has been introduced and tested for a 50 mT Halbach-based portable MRI system under different EMI conditions. Reductions in EMI of over 90 % were achieved for both narrow-band and broad-band EMI sources. This simple approach has both advantages and limitations with respect to other methods in the literature. It does not require external sensors or extensive signal processing and can be implemented on a single

receiver console. However, if a system with only one receiver channel is available, the use of a 180° power splitter/combiner does reduce the SNR by ~ 40 %: if two receive channels are available this loss is eliminated.

Data availability

Data will be made available on request.

Declaration of Competing Interest

The authors declare that they have no known competing financial interests or personal relationships that could have appeared to influence the work reported in this paper.

Acknowledgments

This work was funded by H2020-MSCA-ITN-ETN-2019 (NOVA-MRI 859908) and a Horizon 2020 ERC Advanced Grant (670629).

References

[1] C.Z. Cooley, J.P. Stockmann, B.D. Armstrong, M. Sarracanie, M.H. Lev, M.S. Rosen, L.L. Wald, Two-dimensional imaging in a lightweight portable MRI scanner without gradient coils, Magn. Reson. Med. 73 (2) (2015) 872–883.
[2] C.Z. Cooley, M.W. Haskell, S.F. Cauley, C. Sappo, C.D. Lapierre, C.G. Ha, J.P. Stockmann, L.L. Wald, Design of sparse halbach magnet arrays for portable MRI using a genetic algorithm, IEEE T Magn 54 (1) (2018).
[3] P.C. McDaniel, C.Z. Cooley, J.P. Stockmann, L.L. Wald, The MR Cap: a single-sided MRI system designed for potential point-of-care limited field-of-view brain imaging, Magn. Reson. Med. 82 (5) (2019) 1946–1960.
[4] C.Z. Cooley, P. McDaniel, J. Stockmann, S.A. Srinivas, S.F. Cauley, M. Sliwiak, C. Sappo, C.F. Vaughn, B. Guerin, M.S. Rosen, M.H. Lev, L.L. Wald, A portable brain MRI scanner for underserved settings and point-of-care imaging. arXiv:200413183 [eessIV], 2020.
[5] T. O'Reilly, W.M. Teeuwisse, A.G. Webb, Three-dimensional MRI in a homogenous 27 cm diameter bore Halbach array magnet, J. Magn. Reson. 307 (2019).
[6] B. de Vos, J. Parsa, Z. Abdulrazaq, W.M. Teeuwisse, C.D.E. Van Speybroeck, D.H. de Gans, R.F. Remis, T. O'Reilly, A.G. Webb, Design, characterisation and performance of an improved portable and sustainable low-field MRI system, Front. Phys.-Lausanne 9 (2021).
[7] Y.L. Liu, A.T.L. Leong, Y.J. Zhao, L.F. Xiao, H.K.F. Mak, A.C.O. Tsang, G.K.K. Lau, G. K.K. Leung, E.X. Wu, A low-cost and shielding-free ultra-low-field brain MRI scanner, Nat. Commun. 12 (1) (2021).
[8] A.M. Prabhat, A.L. Crawford, M.H. Mazurek, M.M. Yuen, I.R. Chavva, A. Ward, W. V. Hofmann Jr, N. Timario, S.R. Qualls, J. Helland, C. Wira, G. Sze, M.S. Rosen, W. T. Kimberly, K.N. Sheth, Methodology for low-field, portable magnetic resonance neuroimaging at the bedside, Front. Neurol. (2021) 12.
[9] K.N. Sheth, M.H. Mazurek, M.M. Yuen, B.A. Cahn, J.T. Shah, A. Ward, J.A. Kim, E.J. Gilmore, G.J. Falcone, N. Petersen, K.T. Gobeske, F. Kaddouh, D.Y. Hwang, J. Schindler, L. Sansing, C. Matouk, J. Rothberg, G. Sze, J. Siner, M.S. Rosen, S. Spudich, W.T. Kimberly, Assessment of brain injury using portable, low-field magnetic resonance imaging at the bedside of critically Ill patients, JAMA Neurol. 78 (1) (2021) 41–47.
[10] M.H. Mazurek, M.M. Yuen, B.A. Cahn, M.S. Rosen, K.T. Gobeske, E.J. Gilmore, D. Hwang, F. Kaddouh, J.A. Kim, G. Falcone, N. Petersen, J. Siner, S. Spudich, G. Sze, W.T. Kimberly, K.N. Sheth, Low-Field, Portable Magnetic Resonance Imaging at the Bedside to Assess Brain Injury in Patients with Severe COVID-19, Neurology 96 (15) (2021).
[11] M.H. Mazurek, B.A. Cahn, M.M. Yuen, A.M. Prabhat, I.R. Chavva, J.T. Shah, A.L. Crawford, E.B. Welch, J. Rothberg, L. Sacolick, M. Poole, C. Wira, C.C. Matouk, A. Ward, N. Timario, A. Leasure, R. Beekman, T.J. Peng, J. Witsch, J.P. Antonios, G.J. Falcone, K.T. Gobeske, N. Petersen, J. Schindler, L. Sansing, E.J. Gilmore, D.Y. Hwang, J.A. Kim, A. Malhotra, G. Sze, M.S. Rosen, W.T. Kimberly, K.N. Sheth, Portable, bedside, low-field magnetic resonance imaging for evaluation of intracerebral hemorrhage, Nat. Commun. 12 (1) (2021) 5119.
[12] J.Z. Li, Z.D. Nie, Y.H. Liu, L. Wang, Y. Hao, Evaluation of propagation characteristics using the human body as an antenna, Sensors-Basel 17 (12) (2017).
[13] T. O'Reilly, W.M. Teeuwisse, D. de Gans, K. Koolstra, A.G. Webb, In vivo 3D brain and extremity MRI at 50 mT using a permanent magnet Halbach array, Magn. Reson. Med. (2020), https://doi.org/10.1002/mrm.28396.
[14] S.A. Srinivas, S.F. Cauley, J.P. Stockmann, C.R. Sappo, C.E. Vaughn, L.L. Wald, W. A. Grissom, C.Z. Cooley, External dynamic interference estimation and removal (EDITER) for low field MRI, Magn. Reson. Med. 87 (2) (2022) 614–628.
[15] D.O. Walsh, Multi-channel surface NMR instrumentation and software for 1D/2D groundwater investigations, J. Appl. Geophys. 66 (3–4) (2008) 140–150.
[16] M. Muller-Petke, Non-remote reference noise cancellation - using reference data in the presence of surface-NMR signals, J. Appl. Geophys. 177 (2020).
[17] D.V. Trushkin, O.A. Shushakov, A.V. Legchenko, The potential of a noise-reducing antenna for surface Nmr groundwater surveys in the earths magnetic-field, Geophys. Prospect. 42 (8) (1994) 855–862.
[18] J.J. Larsen, E. Dalgaard, E. Auken, Noise cancelling of MRS signals combining model-based removal of powerline harmonics and multichannel Wiener filtering, Geophys. J. Int. 196 (2) (2014) 828–836.
[19] E. Dalgaard, E. Auken, J.J. Larsen, Adaptive noise cancelling of multichannel magnetic resonance sounding signals, Geophys. J. Int. 191 (1) (2012) 88–100.
[20] E. Dalgaard, P. Christiansen, J.J. Larsen, E. Auken, A temporal and spatial analysis of anthropogenic noise sources affecting SNMR, J. Appl. Geophys. 110 (2014) 34–42.
[21] D.I. Hoult, R.E. Richards, The signal-to-noise ratio of the nuclear magnetic resonance experiment, J. Magn. Reson. 213 (2) (2011) 329–343.